STUDY ON SYNERGETIC OBSERVATIONS OF EARTH RADIATION MISSION INSTRUMENTS

ESTEC/CONTRACT NO.12068/96/NL/CN

Executive Summary Report

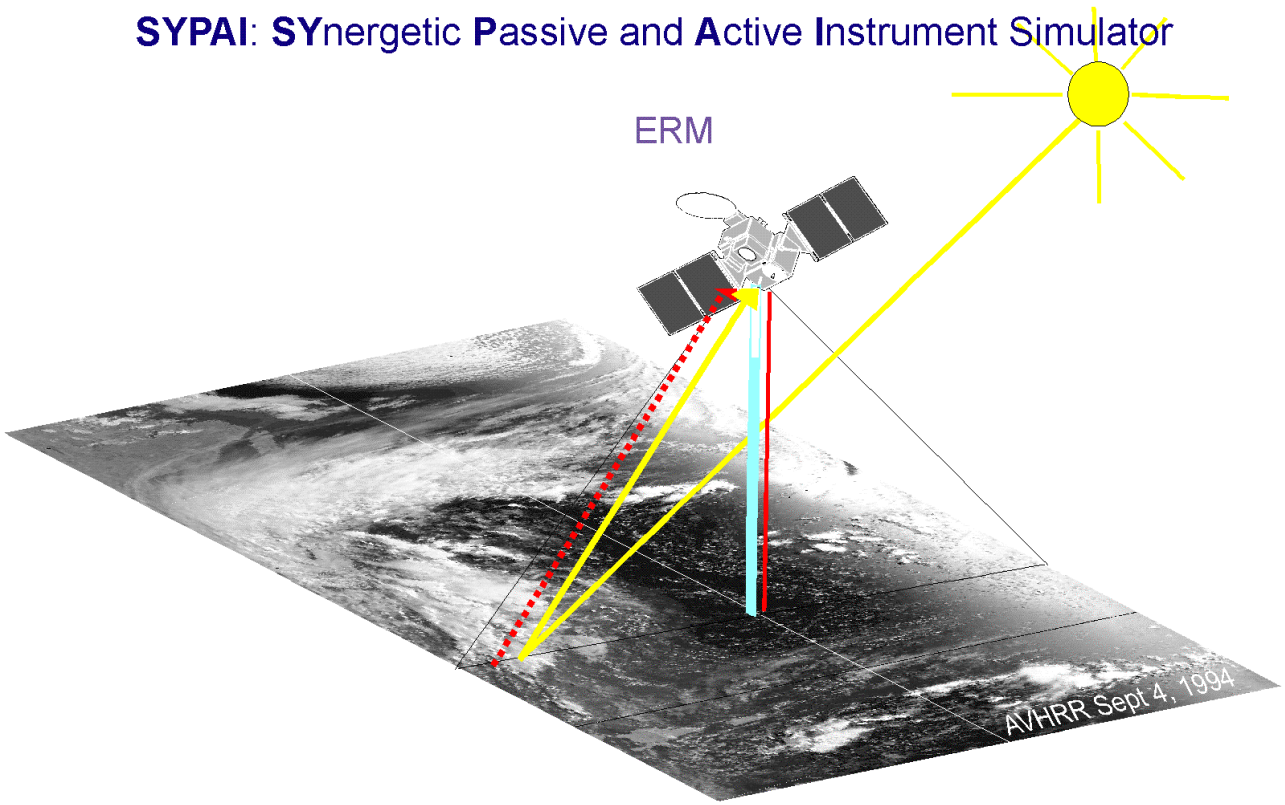

European Space Agency Contract Report

The work described in this report was done under ESA contract. Responsibility for the contents resides in the authors or organization that prepared it.

STUDY ON SYNERGETIC OBSERVATIONS OF EARTH RADIATION MISSION INSTRUMENTS

ESTEC/CONTRACT NO.12068/96/NL/CN

EXECUTIVE SUMMARY REPORT

Submitted to :

Paul Ingmann
Scientific Authority
European Space Research and Technology Centre
2200 AG Noordwijk
Keplerlaan 1, 2201 Az Noordwijk
The Netherlands

Prepared by:

M. St-Onge, R. Girard and P.S. Park
MPB Technologies Inc.
151 Hymus Blvd.
Pointe Claire, Quebec
CANADA H9R 1E9

S. Pal, M. Cann, R. Berman, P. Duggan, and D.Donovan
CRESTech, 4850 Keele St.
North York, Ontario
CANADA M3J 3K1

J.P. Blanchet, M. Larocque and W. Szyrmer
Département de Physique
Université du Québec à Montréal
Case postale 8888, Succursale A
Montréal, Québec
CANADA H3C 3P8

L. Garand,
AES/Canadian Meteorological Center

Zhanqing Li,
Canada Center for Remote Sensing

Date: March 31, 2000
MPBT 512SR007, Version 1.0

ESA STUDY CONTRACT REPORT

ESA CONTRACT No *12068/96/NL/CN*	SUBJECT ***Study on Synergetic Observations of Earth Radiation Mission Instruments***		CONTRACTOR *MPB Technologies Inc.*
ESA CR (P) No **4295**	STAR CODE	No of Volumes 3 This Volume is No 1	CONTRACTOR'S REFERENCE

ABSTRACT:

In the context of Earth Radiation Mission (ERM), a simulator (SYPAI) has been developed in order to perform synergetic studies for the simultaneous exploitation of spaceborne instruments. Different realistic datasets representing the various atmospheric conditions of interest have been generated. As a part of SYPAI, four software tools have been developed to allow accurate simulation of the performance of the proposed instruments: a Cloud Profiling Radar, a Backscatter Lidar, a Broad-Band Radiometer and a Vis/IR Imager. In the course of this study, various forward and retrieval algorithms have been reviewed and implemented for each instrument. Non-synergetic results are presented where characteristic parameters measured by each instrument are shown for South-North satellite trajectory (some W-E trajectories are also presented). Synergetic potentialities have been explored: synergetic algorithms (based on cloud edge detection and ratio of backscatter reflectivities) have been used to evaluate the complementarity and cooperability between the active instruments (Radar and Lidar). A comparison of retrieved data set has also been done against the original input data in terms of TOA flux – surface radiative forcing and heating rates (RAM scheme). In the case of split mission scenario, the spatial separation and time delay requirement aspects have been evaluated.

Names of authors:

M. St-Onge, R. Girard and P.S. Park (MPB Technologies Inc, Canada)
J.P. Blanchet, M. Larocque and W. Szyrmer (Université du Québec à Montréal, Canada)
S. Pal, M. Cann, R. Berman, P. Duggan and D.Donovan (CRESTech, Canada)
L. Garand (AES/Canadian Meteorological Center), *Zhanqing Li* (Canada Center for Remote Sensing)

NAME OF ESA STUDY MANAGER *Dr. Paul Ingmann* DIV: *Earth Science* DIRECTORATE:	ESA BUDGET HEADING

Table of Contents

1. Introduction

1.1 Introduction

This document is the Volume 1 of the Final Reports produced for ESTEC Contract No. 12068/96/NL/CN, "Study on Synergetic Observations of Earth Radiation Mission Instruments". It contains executive summary of the activities performed by MPB Technologies Inc (MPBT, prime contractor), Université du Québec à Montréal (UQAM) and Center for Research in Earth and Space Technology (CRESTech, formerly ISTS).

The aim of this project is to produce a software tool that allows accurate simulation of the performance of a proposed suite of instruments for the Earth Radiation Mission. The study work has been divided into three tasks. Task 1 was to review the forward models and retrieval algorithms for the different instruments, prepare an input dataset for atmospheric modeling and develop simulation scenarios. Task 2 activities consisted of input dataset preparation, module development, code integration and tests for the simulation tool. Then, in Task 3, simulation of the instrument responses for different scenarios and analysis of the results were carried out. An extesion to the contract was approved to improve on synergetic algorithm, additional simulation scenario including the split mission. It involved three additional scientific experts added to provide consultation in formulating the synergetic algorithms.

1.2 ERM Background

In recognition of the importance of a better understanding of the atmospheric processes involved in the Earth radiation budget, ESA prepared an Earth Radiation Mission (ERM) in consultation with the Earth observation community. Its mission objectives are to advance the understanding of the role of the Earth radiation budget with respect to the following climatological (or process) issues:

- In maintaining the present climate.
- In governing the amplitude and evolution of large scale climate anomalies.
- In determining how climate changes in response to perturbations.

The above objectives require a complete picture of the 3-dimensional structure of the radiative transfer within the atmosphere and at the surface for the atmospheric volume probed at the time of measurement. In order to provide a full set of necessary climatological data, four core instruments are proposed [ERM, 1996];

- A *backscatter lidar* (BL) to observe the characteristics of aerosol, thin cloud layers and cloud top heights;
- A *cloud profiling radar* (CPR) for the retrieval of the geometrical properties of thick clouds, LWC/IWC distribution within clouds, and precipitation;
- A *broadband scanning radiometer* (BR) to measure shortwave (SW) and longwave (LW) fluxes at top of atmosphere (TOA).
- A passive VIS/IR high resolution cloud imager (CI) with a resolution compatible with backscatter lidar and CPR to validate the representativity of measured cloud fields by the active instruments and provide complementary measurements of cloud optical properties, horizontal structure and cloud top

temperature.

In order to define the observational requirements for the instruments proposed above, the accuracy requirements for the key parameters is derived from the impact they have on the radiation budget at the top or at the bottom of the atmosphere. The accuracy requirements at TOA and within the atmosphere are listed in Tables 1.2-1 and 1.2-2 respectively.

Table 1.2-1: Required accuracy for SW and LW fluxes at the top of atmosphere.

Measurement objective	**Spatial scale**	**Temporal scale**	**Accuracy of SW and LW fluxes at TOA (Wm^{-2})**
Global radiance balance	Global	seasonally	1 - 3
Regional climate variability	100-250 km	monthly	2 - 5
Detailed process studies	35 - 250 km or pixel	composites or instantaneous	5 - 10

Table 1.2-2:Desired rms accuracy of parameters to be measured within the atmosphere.

Parameter	Spatial scale	Desired accuracy (detection limit)
SW and LW flux at TOA	50 x 50 km^2	5 – 10 Wm^{-2}
Layer tops/bottoms	50 x 50 km^2	0.2 km
Cloud fractional coverage	50 x 50 km^2	5 %
Cloud optical thickness	50 x 50 km^2	0.1(detection limit)
Liquid/ice water content	50 x 50 km^2	0.2 gm^{-3} (detection limit)
Effective particle size	50 x 50 km^2	(to be defined)
Stratospheric aerosol optical thickness	1000 x 1000 km^2	0.1
Boundary layer aerosol optical thickness	50 x50 km^2	0.1
T/H_2O profile	50 x 50 km^2	1 K/10% rel. humidity
Surface emissivity	50 x 50 km^2	0.03

Acknowledgements

We would like to thank Si-Chee Tsay who has developed the latest version of DISORT method, Jeffrey R. Key who has allowed us to use one implementation of this code, STREAMER, and Lubos Spacek.

We would like to thank also Anthony Illingworth, Franz Burger and André van Lammeren for their contribution toward improved algorithm development and especially in synergetic algorithms in the course of this study.

2. Simulation Tool Description

2.1 Simulation tool Structure

The simulation tool developed is denoted as the SYPAI which is derived from "SYnergetic Passive and Active Instrument simulator". Its overall schematic diagram is shown in Figure A-1 (Appendix A) which consists of the following main modules:

- Input Data Set: original data containing 3 dimensional information on the state of atmosphere and 2 dimensional field for TOA radiances.
- Active ERM Instrument Measurement: modeling of radar and lidar measurements.
- Passive ERM Instrument Measurement: forward modeling of BBR and cloud imager.
- Non-synergetic Retrieval: retrieval algorithms based on measured data of each individual instrument, i.e., no synergism between the instruments included.
- Synergetic retrieval: improved algorithms that take account of available data from radar and lidar, and between active and passive instruments.
- Radiative transfer code: STREAMER
- Radiation Analysis Module (RAM)

From global NMC (US National Meteorological Centre) objective analysis, the Canadian Regional Climate Model (RCM) is run in forecast mode to simulate the temporal evolution of the atmosphere in the domain. The RCM calculates realistic 3D cloud structures, temperature, water vapour and winds. These basic prognostic variables are then analysed in a post processing diagnostic program called CLDPROG. In turn CLDPROG computes the 3D and 2D basic data for SYPAI referred to as the "input dataset". An intermediate program called STRUCTUR assembles the individual files of each variable into the single structured "input dataset" for SYPAI. This input dataset defines the atmosphere as a single static "frame", the scenarios described in the previous section.

SYPAI runs in two modes. First, when spectral radiance is not yet available (RUN #1), the model calls STREAMER [Key, 1996], a version of DISORT [Tsay et al., 1989, 1990]. The STREAMER code is used without modification and according to the author's documentation. Due to computational time limitation, radiance is computed from the discrete ordinate method set to four streams only. Yet, this calculation on a 80x80 grid frame requires about 5 days of CPU time on a fast server (SGI Origin 200).

From STREAMER, the computation of 129 spectral intervals of radiance is stored into a radiation dataset (`Radiance_129_full.dau`) as a full spectrum of radiance so any radiance sub intervals can be extracted for particular definition of passive instruments. In this manner, individual subset of radiances are extracted assuming BBR ranges (0.2-4.0μm and 4.0-100μm) and AVHRR Imager 5 spectral intervals.

When spectral radiance is available, i.e., in the second mode (RUN #2), SYPAI calls directly individual instruments and the appropriate radiance field to calculate measured signals for each instrument using the forward modules. From these signals, retrievals for geophysical parameters are performed at two levels; the non-synergetic (Level 1) and synergetic (Level 2) retrievals. Non-synergetic retrieval is done for each instrument separately without assuming existence of data from other instruments whereas the

synergetic retrieval algrorithms combine the data obtained from all the instruments.

Comparison and analysis is done at two levels corresponding to cloud physical parameters (cloud top and bottom heights, LWC, IWC, Optical thickness, Effective particle sizes, etc.) and radiation parameters (TOA and surface radiative fluxes and vertical heating rates). RAM is introduced for anlysis and comparison at radiation parameter level. Description of major modules is given in the following subsections.

2.2 Input data set

The realistic dataset representing the various atmospheric conditions of interest are generated and analyzed. The horizontal spatial resolution range from ultra-high resolution of 25m, medium resolution of 7 km and low resolution of 50 km. The following types of weather conditions are simulated :

- North Atlantic Low Resolution (50km); Mature Synoptic Storm
- North Atlantic Medium Resolution (7km); Frontal and Jetstream Clouds
- Mexico Dataset (10km); High Altitude Convective Cirrus
- CLARE Dataset (50km); Intensive Experiment Site
- LITE (100km); Large Scale Continental Aerosol
- Ultra High Resolution (25m); Marine stratus, Broken Arctic Stratocumulus, and Fair Weather Cumulus

Low to medium resolution datasets are used for simulation of ERM instruments whereas the ultra-high resolution dataset is used for simulation of split mission scenario.

The input dataset obtained is by running the Canadian Regional Climate Model (RCM) to different resolutions of 50, 7 and 1-km in 3D and 25m in 2D, all with a fixed 80 by 80 grid mesh. It contains all the relevant parameters defining the atmospheric and surface conditions.

2.3 Cloud Profiling Radar (CPR) Instrument models

2.3.1 CPR Forward model

The forward model computes the received power backscattered from clouds and surface. The CPR measures the total backscatter power as a function of range. Only incoherent power measurement is modeled. The cloud backscatter power is found by subtracting an estimate of noise from the total return. The cloud return power is usually so low compared to the receiver noise level that a large number of pulses must be averaged to reduce statistical error on the estimate. The normal mode of operation consists in measuring the return power from a number of pulses corresponding to a nadir looking radar.

The total power return to the radar denoted $P_T(r)$, is given by:

$$P_T(r) = P_{cl}(r) + P_N(r) + P_{surf}(r) + P_{rain}(r) ,$$

where $P_{cl}(r)$ is the power returned from clouds at range r, $P_N(r)$ is the noise power, $P_{surf}(r)$ is the

surface return power and $P_{rain}(r)$ is the rain return.

For a space-borne non-coherent radar, the measured backscattered power from clouds is given by the radar equation for extended target. Specializing for the case of a non-coherent radar with a narrow Gaussian antenna beam, the return power from the clouds is given by:

$$P_{cl}(r) = \frac{P_o (G_o \lambda)^2 \theta_3 \phi_3 \eta(r) c \tau \exp(-2\gamma(r))}{2^{10} \pi^2 r^2 \ln 2 L_T L_R L_{Atm}}$$

where:

P_o	is the transmit power,
λ	is the wavelength,
G_o	is the antenna gain,
θ_3	is the beamwidth is the along-track direction,
ϕ_3	is the beamwidth in the azimuth direction,
$\eta(r)$	is the volumetric cross-section,
$\gamma(r)$	is the one-way attenuation along the path,
L_T	is the transmitter loss,
L_R	is the receiver loss and
L_{Atm}	is the atmospheric (2-way) attenuation.

The most critical cloud physical parameter in the above equation is the cloud backscattering scross-section $\eta(r)$ which is normally expressed in terms of radar reflectivity Z or dBZ. The reflectivity is computed using two different methods; the drop size distribution model (DSD) based, and semi-empirical based models. The DSD based method uses the relation derived for Z assuming modified gamma distributed spherical DSD in Rayleigh limit. In this case, Z is proportinal to R_e^3 *M where R_e is effective droplet radius and M is LWC. For ice clouds, an equivalent sphere technique is used by introducing a correction factor to take account of crystal shapes. The effective radii are calculated using the Fouquart [Fouquart 1985] and Wyser [Wyser 1998] models for liquid and ice clouds respectively which are available from input dataset. The phase of cloud (i.e., liquid/ice fraction) is determined usign the relation introduced by Rockel et al. [Rockel 1991]. The DSD based method gives more realistic values for the ice cloud reflectivities since it depends on temperature. Previously, using semi-empirical relation gave an over-estimate of the reflectivities for high altitude ice clouds where temperature is expected to be quite low.

The attenuation of radar signal through clouds is calculated using a semi-empirical relation which depend only on liquid water content, i.e, no attenuation for ice clouds. Corrections are applied for the fractional cloud cover and multilayer clouds. The contribution of rain is also included for both the reflectivity and attenuation calculation. Only water vapor are taken into account in the determination of the clear-air atmospheric attenuation. The noise correlation is modeled along the time axis and fluctuations are added in the models used. In order to enhance the cloud detection, the measured reflectivities are integrated and noise power which is derived separately is subtracted, and a threshold is applied in the post-processing step.

Main radar system parameter are listed in Table 2.3-1.

Table 2.3-1: Radar Instrument Parameters.

Parameter	Unit	MACSIM Value	CloudSat Value	Dornier (99/03/09)
Frequency	GHz	95.0	94.7	94.05
PRF	Hz	4200.	4700/2	5309.68
Transmit Peak Power	Watt	1500.	1500	1500.
Resolution	meter	500.0	500	500.0
Transmit Loss	dB	1.03	1.0	1.38
Gain	dB	66.2	63.3	63.9
Beamwidth	degree	0.086	0.012	0.145
Receive Loss	dB	1.0	0.6	1.1
System Noise Temperature	kelvins	466.0	500	945.0
Vertical Sampling Distance	meter	500.0	500	500.0
Horizontal Sampling Distance	meter	1000.0	1000	1000.0

2.3.2 CPR Retrieval Algorithms

A list of retrieval algorithms implemented for cloud radar is given in Table 2.3-2. Different retrieval algorithms are explored and a semi-empirical relation is employed with compensation for attenuation and assuming mixed-phase clouds. Only synergetic algorithms that use both lidar and radar measurements have been implemented.

Table 2.3-2: Retrieval algorithms implemented that use CPR forward model data

Retrieved parameters	Description
Cloud Top and Bottom Detection	Based on the results from cloud detection algorithm, each cloud layer is identified and its top and bottom heights are determined.
Effective (True) Cloud Reflectivities and Cloud Water Retrieval	At most general level, semi-empirical formulation in conjunction with Rockel relation is used to derive the effective (true) reflectivities and LWC/IWC. This is done through iteration method starting from top of the atmosphere.
Effective Droplet Radius for Ice Clouds	Forward model data from radar and lidar are used to compute Lidar/Radar ratio which is independent of IWC and function of only effective radius
Cloud Emissivity	From liquid/ice water path (L/IWP) values, emissivities of mixed clouds are computed

2.4 Lidar Instrument Models

2.4.1 Lidar Forward Model

The backscattered power for lidar is computed as a function of range by the lidar equation,

$$P_T(r) = C\frac{\beta_\pi(r)}{r^2}e^{\left[-2\int_0^r \alpha(r')dr'\right]} + P_N + P_{back}$$

where,

C is the instrument constant.

β_π is the total atmospheric backscatter coefficient.

r is the range from the lidar.

α is the total atmospheric extinction coefficient.

P_N is the electronic noise power.

P_{back} is the background power

The system constant includes parameters related to the transmitter and receiver that presumably do not change over an operational time window. The background signal refers to power registered by the lidar receiver that is due to the detection of photons from sources other than backscattered laser light. In the case here, the main source of background light will be scattered sunlight from the earth's surface and atmosphere. As such, the background will depend on the solar angle, the surface type and the cloud cover. There are several sources of noise in the measured signal. Just as a filter-width allows extraneous background photons, an equivalent noise-width B permits the noise equivalent currents to contribute to the total signal. The noise current levels have already been worked out for ATLID (private communication with A. Culoma, ESTEC) and the same values have been adopted.

Table 2.4-1: Nadir-looking ATLID system parameters

Signal Energy P_o	100 Mj
Wavelength λ_o	1.064 μm
Telescope Diameter D	0.9 m
Quantum Efficiency η	0.35
Range Resolution Δz	100 m
Bulk Dark Current I_{DB}	1.2 pA
Surface Dark Current I_{DS}	50 nA
Detector gain g	39
Field of View Ψ	540 μrad
Upwelling Radiance aI_B	220 W/m^2/μm (Day) , 0 (Night)
Spectral width $\Delta\lambda_o$	0.28 nm
Excess Noise Factor F	2.3
Optical efficiency T_{opt}	0.4
Receiver efficiency T_{rec}	0.49

The backscattering and extinction coefficients depend on the atmospheric optical characteristics which

consist of three main scatterers; atmospheric molecular, aerosol and clouds. Molecular backscattering and extinction coefficients are related to the atmospheric molecular number density via Rayleigh scattering. The atmospheric molecular density is derived from the temperature and pressure in the input dataset. Since, in general, the lidar vertical resolution is much finer than the RCM vertical resolution, the density at each of the lidar ranges is found by exponential interpolation between the given input dataset levels. The molecular extinction and backscatter profile used in the lidar signal simulation is then found using the resulting 'high-resolution' density profile.

Standard aerosol models (e.g. LOWTRAN type profiles) have been adapted for for aerosol scattering coefficients. For the present study, boundary layer aerosol, free tropospheric aerosol and stratospheric aerosol profiles are carefully combined and detailed Mie calculations were performed for 1064 nm to calculate both the extinction and backscatter coefficients up to the top of the stratosphere. No fixed extinction-to-backscatter ratio for aerosols was utilized. Altitude dependent aerosol backscatter and extinction coefficients thus produced may be read from an ASCII data file. The ability to read in the aerosol data from a simple ASCII data file gives a great degree of freedom in specifying the aerosol properties used in the simulations.

For water cloud extinction and backscatter coefficients at a given wavelength, in general, they are functions of the cloud particle size distribution and the refractive index of the cloud droplets. Since the DSD information is not available in input dataset, it is modelled using the gamma distribution. Then, following Hu and Stamnes [Hu 1993], Mie calculations were performed which is parametrized by two parameters; characteristic radius r_{eff} and width γ. However, it can be shown that cloud scattering coefficients are not sensitive to γ for given effective radius. Hence, a look-up table is used which has been generated as function of effective radius at a fixed value of gamma (γ=10). For the case of ice clouds, an empirical relation proposed by Ebert and Curry relating extinction coefficient α_c as function of IWC and R_{eff} is used to compute the extinction coefficient [Ebert 1992]. Finally, the backscattering coefficient β_c is found by using a lidar ratio of 18 (= α_c/β_c). The relationship between the backscatter and extinction coefficients will depend on the crystal size distribution as well as the crystal sizes and orientation (Hess and Wienger, 1994). The complexity of scattering by non-spherical particles in the optical wavelength region dictates assuming a constant lidar ratio for ice particles. This value was assumed on the basis of research existing in the literature and in the ESA reports ([Ansmann 1992], [Boesenberg 1997], [Kahler 1995]).

For space based lidars multiple scattering is a significant effect. The contribution to the lidar signal will increase with the number of mean free-paths contained in the instantaneous sampling volume. For space based lidars, even with a narrow receiver field-of-view, the sampling volume will often contain many mean-free-paths. In general, for space based lidars the multiply scattered return will be significant for all but the thinnest of clouds [Winker 1994]. A detailed account of multiple scattering effects is considered to be beyond the present scope of this work. However, a multiple scattering correction factor η_{ms} has been introduced into the forward model calculations to approximately account for its effects (i.e., a correction factor on extiction coefficient). Following the work presented in Kahler et. al. [Kahler 1995], a value of 0.50 has been adopted for cirrus clouds and a value of 0.55 for water clouds.

Using the lidar equation, the signal received by the lidar is calculated for each shot. Two contributions to the signal are the background and electronic noise. First the constant background is added to the signal and then a random noise contribution is added as described above. To reduce the effects of the noise

contribution to the signal and improve the lidar signal-to-noise ratio, the return power is averaged over a number of shots. The number of shots is determined by the horizontal resolution required, the laser repetition rate, and the satellite speed.

2.4.2 Lidar Retrieval Algorithms

The retrieval algorithms implemented are summarized in Table 2.4-2.

Table 2.4-2: Retrieval algorithms implemented that use CPR forward model data

Retrieved parameters	Description
Cloud Top and Bottom Detection	Similar to that used by Bosenberg et al. [Bosenberg 1997]
Cloud Optical Depth and Extinction	$\tau_{eff}(r,r_o) = -0.5\times\ln\left(\exp[-2\tau_{eff}(r_o,0)] - \frac{2}{C}\int_{r_o}^{r} S_{eff}(r')r'^2\,P(r')dr'\right)$ $\alpha(r) = \frac{\alpha_{eff}(r)}{\eta_{ms}(r)} = \frac{1}{\eta_{ms}(r)}\frac{d\tau_{eff}(r)}{dr}$

2.5 BBR Instrument Modules

The Broad-Band Radiometer is a scanning instrument designed to measure radiation over a wide wavelength interval in order to obtain the radiation fluxes leaving the Earth at the Top Of the Atmosphere (TOA). The instrument specifications are as shown in Table 2.5-1 for nadir viewing, the Sub-Satellite Position (SSP).

Table 2.5-1 Broad-Band Radiometer Specifications

	Short-Wave Channel (reflected Solar)	Long-Wave Channel (Earth emission)
Spectral pass-band (:m).	0.2 - 4.0	4.0 - 50.0
Dynamic range ($w.m^{-2}.sr^{-1}$)	0 - 450	0 - 130
Absolute accuracy ($w.m^{-2}.sr^{-1}$)	< 1.0	< 0.3
Noise equivalent radiance ($w.m^{-2}.sr^{-1}$)	< 0.3	< 0.1
Field of View (FOV) (km)	∀1000	∀1000
Instantaneous FOV (iFOV) at SSP (km)	48	48
Sampling distance at SSP (km)	30	30
Registration with other instruments	no requirements	no requirements

An algorithm is used to convert the raw measurements into instantaneous radiances, including necessary calibration corrections, offsets and gains for a specific time and spatial coordinates. Many of the calibration parameters are obtained from a calibration facility prior to launch. The algorithm can be written (Halyo et al., 1989, Lee et al., 1989, Lee et al., 1996). The filtered radiance can also be expressed in terms of the true, spectral radiance L(λ), the angle dependent spectral response S(λ,Ω), and the angular point spread function P(Ω) by:

$$L(t-\tau) \quad = \quad \int d\Omega\, P(\Omega) \int_0^{\infty} d\lambda\, S(\lambda)\, L(\lambda,\Omega)$$

In order to derive TOA radiation budget, the output radiance is inverted into radiation flux via the expression given below;

$$M_{\lambda}(\Theta,\Phi,t) \quad = \quad \int_0^{2\pi} d\phi \int_0^{\pi/2} d\theta\, L_{\lambda}(\Theta,\Phi,\theta,\phi,t) \sin\theta\cos\theta$$

where Θ and Φ are the colatitude and longitude of the exiting ray, and θ and ϕ the zenith and azimuthal angles respectively. In practice if the measurement of $\boldsymbol{L}_{\lambda}$ at any given geographic location (Θ, Φ) is made for only one view (θ, ϕ) then $\boldsymbol{M}_{\lambda}$ must be inferred from a model. This can be done through a bi-directional reflectance, or "Angular Dependence Model" (ADM). The model developed by Wielicki and Green [Wielicki 1989] has been implemented.

2.6 Cloud Imager Modules

The imager is an across-track scanning instrument which measures the TOA radiation signature in several visible and infrared channels, at moderate spectral resolution. The nominal wavelengths for these channels are chosen in the visible spectral region, where only reflected solar radiation is detected, the middle infra-red, where the radiation is only the thermal emission from the Earth's surface and atmosphere, and the near infra-red where, in the day-time, the detected radiation is a mixture of the two.

The VIS/IR imager simulation and analysis modules were implemented based on the 7 AVHRR channels ranging from the visible to infrared. A small 1kmx1km square foot print was used for testing. From the measured radiances, retrieval for scene temperature and albedo were done using the appropriate channels. Additional analysis for cloud cover has been implemented and tested on a limited scale.

2.7 Radiation Analysis Module (RAM)

One way of assessing the quality of the retrieved data is to compare them with the reference dataset in terms of radiative fluxes and heating rates. This is achieved by calculating radiative transfer (RT) twice: first, using the original dataset and second using the retrieved dataset with or without synergy. The RT is solved using the STREAMER routine in flux mode and based on a standard two-stream method [Key 1998]. Radiative fluxes are calculated with a spectral resolution of 129 intervals as in the DISORT case but only broad band integrated results are examined here. TOA and surface fluxes are extracted for

solar and IR ranges together with the net radiative heating rate profiles and the cloud radiative forcing.

3. Analysis of the Simulated Results

3.1 Non-synergy Simulation Results

Simulations have been performed for all the scenes listed in Section 2.2. The CPR instrument parameters used are the Phase A MACSIM. Types of outputs that can be generated are listed in Table 3.1-1. An example of generated results is shown in Figure A-2 (compilation of all the generated results given in Volume 3 of the Final report). The water content of CLARE50km_16oct1998 input dataset, as used in the forward model, is given in the top panel of the figure. The x-axis is the distance on the ground sampled every 10.0 km. The water content is given in logarithmic scale. To avoid log of zeros, a threshold value of 10^{-7} g/m^3 is imposed such that all water content lower than this value appears white on the display. The magenta and blue dotted points on the display represent the retrieved cloud top and bottom heights respectively, which are the limits of each layer of the CPR detected signal (averaged apparent reflectivity). The top and bottom mean errors are indicated. The error is the mean difference between the retrieved (H_r) and true (H_t) cloud boundaries.

The CPR does not detect a large cloud area above an altitude of 11 km: a difference of -3408 m is observed between the retrieved and the true tops. A certain number of detection limits occur between an altitude of 11 km and 15 km. This missed area has a lower reflectivity than the CPR minimum detectable signal. But, the cloud bottoms are very well detected. The very low mean bottom error (an error of only 55 m is observed) hides the fact that the individual error can have higher values along the trajectory. Nevertheless, we can state that an error smaller than the CPR resolution (500 m) would be acceptable.

The retrieved water content derived from integrated apparent reflectivity field is given in the second panel of the figure. The retrieval algorithm uses compensation for the attenuation along the vertical column and assumes mixed-phase clouds. It considers which fraction of the reflectivity is due to ice and water. All instrument errors are included. The comparison of both fields leads us to two remarks. On the one hand, the retrieved water content is overestimated for altitudes between 3 km and 8 km. On the other hand, it is underestimated for altitudes below 3 km (at ground distances between 2000 km and 2700 km). These areas correspond respectively to high and low apparent reflectivity regions. The apparent reflectivity of thin low cloud layers are underestimated if the vertical cloud size is smaller than the resolution.

The histograms of the lower panels, showing the number of sample against the water content in dB, indicate that the maximum value are approximately 0.25 g/ m^3 and 0.6 g/ m^3 for dataset and retrieved water content respectively. One notes that the minimum water content for both is around 0.0005 g/m^3.

Another way to make the comparison is shown by lower panel of Figure A-3. It gives the integrated water content over each column, which is easier to compare. For the whole trajectory, the CPR measurement of water content is overestimated of -55% (averaged along the horizontal distance) compared with the true value even if a large area of the upper deck cloud is not detected. In this region, the water content is so small that it doesn't make any difference in the integration along the vertical distance. The retrieved value is close to the true integrated water content only between the ground distance of 0 and 1000 km in the ice cloud area. Between 2200 km and 2600 km, the retrieved water

content is lower than the true value. The upper panel shows the one-way specific attenuation integrated over each column. This includes attenuation from clouds and the atmosphere. Up to a ground distance of 1000 km, the attenuation is negligible, as expected. This is ice cloud area. For the rest of the trajectory, the attenuation is small (maximum at 1.2 dB) and it allows the cloud radar to detect most cloud bottoms.

Table 3.1-1Types of Outputs from Cloud Radar Simulation

File Name	Description (Remark)
*Signame*_AUTOCORREL	Auto-correlation of Signame (Done by AUTOCORREL.M program)
AVERZAPP	Average reflectivity field over the radar integration length.
CLOUDVOL2	Cloud volume detected by radar and lidar.
COMPREFFCPR	Comparison of Retrieved Effective Radius with Dataset
COMPREFFICE	Comparison of Ice Retrieved Effective Radius (coming from Lidar/Radar ratio) with Dataset
DIFFWAT	Error in retrieval of the water contents.
DIFFZAPP	Error in measured apparent reflectivity.
EMISSEWC	Emissivity from EWCRET compared to EWC
EMISSICE	Emissivity from Ice Water Content retrieved by Lidar/Radar ratio compared to EWC
EWC	Total water content (Reference value in the dataset). Cloud top and bottom from Radar.
EWCRET	Retrieved water content by the CPR from the reflectivity field.
EWC2SY	Comparison of Cloud top and bottom from Radar and Lidar retrievals with EWC.
IWCRET	Comparison of Ice Retrieved Water Content from Lidar/Radar ratio with EWC.
HAVERZ	Histogram of the apparent reflectivity field. (Reference value without instrument errors).
HEWC	Histogram of the reference value of the water content.
HEWCRET	Histogram of the retrieved water content.
HMEASZ	Histogram of the measured apparent reflectivity by the radar.
HZAPP	Histogram of the apparent reflectivity field.
INTATT	Display of the total attenuation along the path.
MEASZAPP	Measured apparent reflectivity field. (Threshold applied to eliminate detection errors.)
RAIN	Display of the precipitation field along the track.
REFFCPRICE	Ice Retrieved Effective Radius by Radar compared with Dataset.
REFFCPRWAT	Water Retrieved Effective Radius by Radar compared with Dataset.
TEMPER	Display of the temperature field along the track (Superposed to Standard Atmosphere.)
TOPBOT	Retrieved cloud top and bottom for the radar (Compared to reference value.)
TOPBOTSY	Retrieved cloud top and bottom for the radar and the lidar. (Compared to reference value.)
ZAPP	Apparent cloud reflectivity field. (True value without instrument errors)

For many cases, the CPR misses also a large area of the cloud top deck because of the lower apparent reflectivity of this cloud portion. The cases where the cloud top is not detected by the CPR are for cirrus clouds with very small ice crystals resulting from tropical intrusions into mid-latitude air. The water content is retrieved with a relatively good precision in the detected area given that all the instrument errors and noise are included in the retrieval. Some of the key results obtained with CPR operating alone are summarized in Table 3.1-2.

Table 3.1-2: Summary cloud retrieval performance with CPR operating alone.

	Clare 50 km	Clare 7 km	Mexico10km	MAP50
Cloud Top/Bottom	Upper half of the upper deck missed:	Upper half of the upper deck: mean	Top and bottom detected	Top and bottom detected

	mean error 3.5 km	error: 4.2 km		
WC (column integrated)	14 % overest. 55% overest.	o.k.. in average 53% overest. in low WC	24 % underest.	31% underest.
Effective Radius (Horizontal averaged)	Excellent	Excellent	?	Water: good Ice: 1-3 overest.
Emissivity	Right half ~ 1.0	Whole cloud ~ 1.0	< 0.5	Right half ~1.0

From the above results the following conclusion may be drawn for the case of CPR non-synergy simulation:

- For Clare-scene type of clouds, cloud top detection is poor and synergy with lidar is clearly required. Also from emissivity data, missed clouds are expected to be radiatively important.

- For WC retrieval, it is accurate within ±50%. Whether this can be improved by synergy with lidar is to be investigated.

- Effective radii are well retrieved for Clare scenes. Quite poor results were obtained for ice clouds in MAP50km scene. It would be interesting to investigate whether, this shortcoming can be improved by exploiting synergism with the lidar.

For the same set of scenes, lidar simulations were carried out. The simulated parameters include extinction, backscatter coefficients and optical depth. In all the cases investigated, the cloud top is extremely well detected. Cloud bottom and multi-layer cloud tops and bottoms are also well detected given sufficient pulse penetration. However much of the liquid cloud bottoms are not seen. Detailed cirrus cloud structure is detected to an optical depth of 1 whereas dense water cloud tops are detected to an optical depth of 4.

Within the assumption of a constant lidar ratio, backscatter and extinction are also well retrieved. The retrieval algorithm is unstable for dense cloud structures at high optical depth and is an area in which further development could extend the retrievals to higher optical depths. Further work could produce a more detailed model for the important effect of multiple scattering. At small optical depths (i.e. clear sky conditions), tropospheric aerosols are also shown to be detected. This area also requires further exploration.

The BBR simulation and analysis were also carried out. Default in the simulation is two channels, SW and LW, as required by the analysis module, but an additional two may be accommodated. Although amplifier gains and off-sets and non-linearity may be specified these are not used as no calibration option has been implemented. The footprint shape and size can be user specified and has been tested with a diamond shape. An occasional problem arises if the footprint lies partially outside the model grid but normally this is handled correctly. Outputs from the analysis on a pixel by pixel basis consist of the scene and the deduced TOA fluxes for SW and LW radiation. The TOA fluxes are calculated using ERBE ADMs. The MLE method cloud identification algorithm has been tested and works although

some tuning of the parameters is required.

For Vis/IR Cloud Imager, only test level simulation has been done using the Sept. 5, 1994 scene over an 80x80 grid with 50km pixel size. With this data set we were able to demonstrate that the code behaved as expected and produced the desired data products. The Vis/IR imager has seven channels. For each of these channels the raw radiances were determined by orbiting the satellite over the scene and performing a set of simulated measurements. The track was restricted to the middle of the grid by the angular dependence of the radiances.

3.2 Synergy Pathways and Simulation

Due to lack of synergetic algorithms including the passive instruments, the synergy analyses were carried out only between the active instruments. With regard to study of synergism between the active instruments, one must distinguish the following two types of synergetic relations:

- Complementary synergy
- Cooperative synergy

Complementary synergy requires a minimum overlap between radar and lidar measured data each instrument providing full information for one part of the whole scene. In this way when they are put together, maximum amount of information is available for the whole scene. For example, this type of synergy is required for cloud top and bottom retrieval. On the other hand, the cooperative synergy requires a maximum overlap between radar and lidar measured data which means twice more information is available for synergetic retrieval of geo-physical parameters.

It is clear that if only complementary synergy is required, one can relax significantly the sensitivity requirements for the instruments whereas the cooperative synergy demands the optimal sensitivity for both instruments. However, the application would be a compromise between these two types of instrument collaboration. Some parameters require cooperative synergy while others require complementary synergy.

As the first key result of the simultaneous exploitation of the two active instruments, the ability of radar sensor to detect through the thick layer down to the cloud bottoms assisted by the high sensitivity of lidar sensor for cloud top detection is clearly demonstrated. An example is shown in Figure A-4. The simulations show that the combined cloud volume is retrieved at nearly 100% over the trajectory by both instruments except CLARE07km_16oct1998 where a 1 km layer remains undetected by lidar for an horizontal ground distance up to 300 km.

The detection of thin cloud layers with cloud vertical extent smaller than 500 m is not well performed by CPR mainly because of its lack of vertical resolution. But, the detection is well done by the lidar instrument, due to higher resolution (100 m), when higher cloud decks do not absorb the signal. Thus, because of its good penetration, the radar signal can identify the boundary of low altitude cloud decks and, when a good accuracy is needed to detect finer cloud structure, lidar measurement should be taken. This is an important aspect of complementarity between the instruments.

Effective radius retrieved by lidar/radar technique was also investigated. This technique exploits another

aspect of synergy; the joint detection of the sensors or cooperative synergy. The comparisons show an overestimation to 40% and 80%. More complex synergetic retrieval algorithms, developed elsewhere during the course of this study, have estimated retrieval errors between 30 to 40% for the IWC and effective radius.

3.3 Radiation Level Analysis

For all the simulation scenarios, a comparison of retrieved data set has been done against the original input data set using the RAM technique described in Section 2.7. This method compares the two data sets in terms of TOA - surface cloud radiative forcing and heating rates. Comparisons have been done between clouds detected only by radar against the case where the complementary synergy is fully exploited (see Figure A-5 for an example of computed outputs). In the latter case, the lidar/radar technique is employed for the joint cloud detection and parameters retrieved from radar are used for cloud decks detected by radar only. Outside this region (cloud decks detected by lidar), extrapolation of prescribed particle size and water content or, in some cases, a climatological prescription based on the temperature gives a first order estimation for the effect of cloud on radiation. A summary of the results for cloud radiative forcing is given in Table 3.3-1.

Table 3.3-1 Differences between retrieved and original datasets for Cloud Radiative Forcing at TOA / Surface (W/m^2)

		Thin high cloud Clare16oct/SN (GP1-GP22)	Thin high cloud Clare14oct/WE (GP1-GP18)	Thick cloud Clare16oct/WE (GP20-GP40)	StratoCumulus Clare16oct/WE (GP1-GP20)
Radar detection only	LW	10 / 40	-10	-20 / 5	0 / 5
	SW	-60 / -40	-10	-20 / -10	0 / -5
Joint synergy	LW			-30 / -50	0 / 10
	SW			100 / 70	10 / 40
Complementary synergy	LW	10 / 60	-5	5 / 5	20 / 5
	SW	-10 / 10	0	-10 / 0	-20 / -25

The combined instrument detection show a general improvement of the flux balance and heating rate profile measurements whose main results can be summarized as

- the TOA radiative contribution of thin high cirrus, that are not detected by radar but detected by lidar, seems small (roughly 10 W/m^2), but it plays an important role in reaching the accuracy required for cloud process study,

- in order to reduce the radiative flux uncertainties, lidar retrieval is to be improved mostly by development of adequate retrieval algorithms,

- the simulations show that the retrieval of ice-liquid water phase is an important factor for the calculation of radiative heating rates and consequently for radiative fluxes also. Its uncertainty can be responsible for large errors in the total results. One important issue in the definition of ERM specification is to consider adapting the requirements of the mission to allow for the evaluation of water phase,

- another difficulty identified in this investigation is the distinction between clouds and aerosols for optical depth around unity. The false identification of cloud results in large errors on the radiation calculation. The final synergetic retrieval algorithms must take proper account of this difficulty,

- in some cases, where the radar retrieves most of the cloud volume (e.g., MAP cases) the single instrument application is generally adequate. However, this may be exceptional among the diversity of possible conditions. For instance low water clouds are often poorly detected by radar alone. In that case the lidar is essential to identify clouds. The lidar is also important for providing higher resolution details of the cloud structure and can improve on the definition of cloud boundaries.

The main limitation of this study is therefore the lack of available retrieval algorithms to fully use the information provided by all instruments. In spite of this limitation, the current simulation demonstrates that the two active instruments are necessary to retrieve adequately the total cloud volume (complementary synergy). Even with this limitation the accuracy of the retrieval of the TOA radiative flux density is in the order of 10 Wm^{-2} at synoptic scales, confirming the overall instrument complement specification.

3.4 Split Mission Simulation

In the context of a non co-located instrument measurements (split mission), sumulations have been carried out using the 25m high resultion and 50km CLARE50km low resolution datasets. The auto-correlation results show that the correlation distance is, as expected, closely related to cloud size and mostly to the integration length of cumulative signal. An important consequence is the limitation in the resolution of the measurements. As the sampling distance is smaller, the correlation length decreases because of the multifractal nature of turbulent clouds limiting the space coherence and, at the same time, the return signal is noisier and the sensitivity detection is lower. The choice of the integration length and the resolution must be carefully balanced with instrument sensitivity.

Main results are summarized in Table 3.4-1. Over a large uniform cloud deck, the correlation length can still seem acceptable. But, over a cloud scene presenting a larger variability, the correlation length reduces at distances as low as the data resolution for radar (1 km). For lidar, where the horizontal resolution is 200 m, the correlation length is slightly better with about 0.5 km because its better cloud top detection. In this case, the retrieval of a fine cloud structure would not be accurate if the instruments are not co-located on the same platform.

Table 3.4-1: Auto-correlation lengths for radar/lidar

	CLARE50km_16oct		**STRATOCUMUL**
	Resolut= 20 km	Resolut= 2 km	Resolution= 1 km
Main Cloud Deck (7-9 km alt) Uniform over 2000 km	300 km / 1000 km	150 km	
Upper deck (9-11 km alt) Uniform over 1000 km	100 km / 500 km	50 km	
Low Water cloud decks	20 km / 50 km		1 km / 0.5 km

4. Conclusions

An executive summary of the results obtained during the course of the contract is presented. Materials summarized in the report include all the key results from the previous technical reports as well as the new simulation results obtained during the additional tasks.

The input datsets were analyzed by comparing with satellite measured data and analyzed extensively. They are shown to be quite realistic in representing the various atmospheric conditions. Instrument forward modelling for radar took account of the latest parametrization relating DSD, LWC/IWC and radar reflectivity. Most of the radar instrument system parameters are incorporated. Lidar forward models included aerosol in addition to molecular and cloud scatterers. Although initial simulated data show that satisfactory results are obtained, more detailed analysis should be done to detemine how well it represents the true lidar measurement. Due to complexity in modelling the passive instrument measurement, no detailed instrument aspects were included in the simulation, i.e., instrument calibration and filter responses.

In terms of retrieval algorithms, non-synergetic algorithms were implemented for the active instruments. Simulated results indicate realistic performances are obtained. For the passive instruments, despite the extensive efforts spent in reviewing and defining the proper algorithms, only some preliminary results on TOA fluxes, albedos and temperature were obtained.

The synergy between radar and lidar was studied in tems of cloud top and bottom detection and effective radius retrievals. Benefits of synergy in cloud top and bottom detection have been clearly demonstrated which require complementary synergism. It would be interesting to investigate further the dependencies in height accuracies as function of instrument sensitivities under synergetic retrievals. Due to lack of available synergy algorithms, full synergy using the data from all four instruments has not been implemented.

Finally, the RAM routine allows the comparison of the final results in terms of radiative fluxes (cloud radiative forcing at top and surface) and heating rates. Detailed analyses were done for all the simulation scenarios to investigate the improvements at radiation level when synergism is implemented.

Split mission scenario is also studied by computing the auto-correlation length using 50km and 25m resolution data sets. Only very preliminary results were obtained and no detailed anlysis was done.

The simulation tool is structured in modular form with all the modules in place so that they can be easily upgraded or replaced. Improvements on the various modules are presently being ccontinued for the following aspects:

- Radiative trandfer code (STREAMER) is replaced with Monte-Carlo based code
- A-band spectrometer instrument algorithms are incorporated into the passive instrument models for CLOUDSAT mission simulation
- Lidar models are upgraded by including the multiple scattering formulation

Due to lack of time and resources, full exploitation of the present simulation tool has not been carried

out within the present contract. With the implementation of passive instrument retrieval routines by modifying one of the many existing algorithms and incorporating the full synergy algorithms, the present simulation tool can be transformed into a useful tool to analyze the ERM as well as the CLOUDSAT missions.

5. References

Ansmann A., U. Wandinger, M., Riebessel, C. Weitkamp, and W, Michaelis, ``Independent measurements of extinction and backscatter profiles in cirrus clouds by using a combined Raman elastic backscatter lidar. Appl. Opts, **31**, 7113-7131 (1992)

Bosenberg, J., R. Timm, and V. Wulfmeyer, ``Study on retrieval algorithms for a backscatter lidar: final report'', ESTEC contract AO/1-2979/95/NL/CN (1997)

Ebert, E., and J.A. Curry, ``A parameterization of ice cloud optical properties for climate models'', J. Geophys. Res., **97**, 3831-3836 (1992)

ERM Report, 1996, "Earth Radiation Mission", Report for Assesment, European Space Agency, ESA SP-1196 (3) (April 1996)

Fouquart, Y., "Radiation in boundary layer clouds", Lab. d'Optique Atmos., Univ. des Sci. et Techniques de Lille, Villeneuve d'Ascq, France IN: World Meteorological Organization, World Climate Program, Geneva, WCP-106, [1985], Appendix D, 40 p. Refs., figs. (WMO/TD No. 75) (1985)

Hu, Y.X., and K. Stamns, ``An accurate parameterization of the radiate properties of water clouds suitable for use in climate models'', J. of Climate, **6**, 728-742 (1993)

Intrieri, J.M. and G. L. Stephens, "A Method for Determining Cirrus Cloud Particle Sizes Using Lidar and Radar Backscatter Technique", Journal of Applied Meteorology, **32**, pp. 1074-82 (1993)

Kahler C., J. Ackermann, M. Wiegner, H., Quenzel, A. Ansmann, U. Wandinger, ``The potential contribution of a backscatter lidar to climatological studies'', ESA contract No, 10722/93/NL/SF (1995)

Key J R, "Streamer. Version 2.4p (Preliminary). User's Guide", Department of Geography, Boston University. Technical Report 96-01, September 8th 1998

Tsay, S.-C., K. Stamnes and K. Jayaweera, "Radiative transfer in stratifies atmosphere: development and verification of a unified model", J. Quant. Spectrosc. Radiat. Transfer, **43**, 133-148 (1990)

Wielicki B A, Green R N, 1989, "Cloud identification for ERBE radiative flux retrieval", J.Appl.Meteorol., **28**, 1133-1146 (1989)

Winker D.M., ``Simulation and modeling of multiple scattering effects observed in LITE data', in Advances in Atmospheric Remote Sensing with Lidar, A. Ansmann, R. Neuber, P. Rairoux, and U. Wandinger Eds., Springer-Verlag, Berlin (1996)

Wyser, K., "The Effective Radius in Ice Clouds", J. Climate, Vol.11, 1993-1802 (1998)

Appendix A

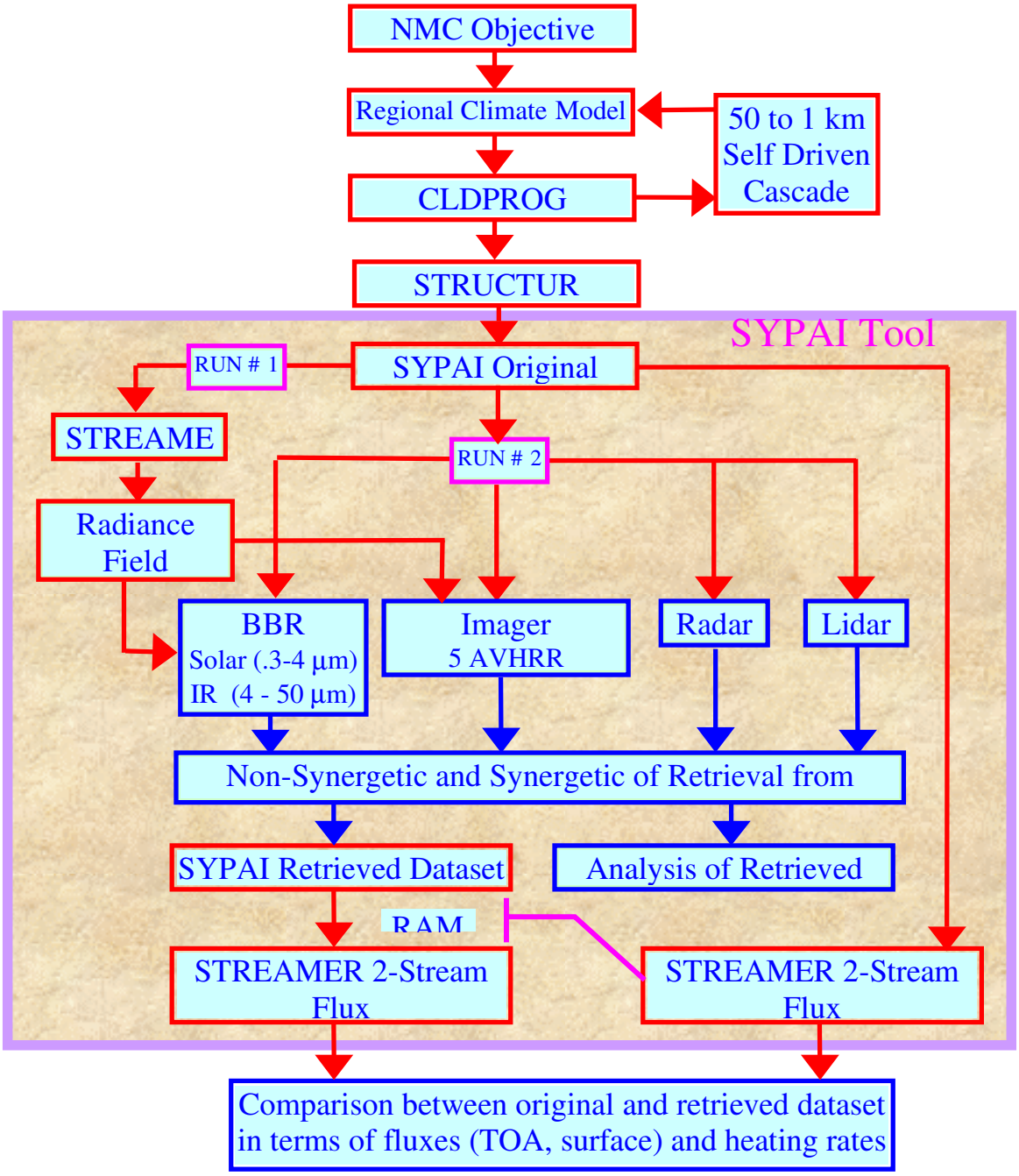

Figure A-1 General structure of the SYPAI simulation tool.

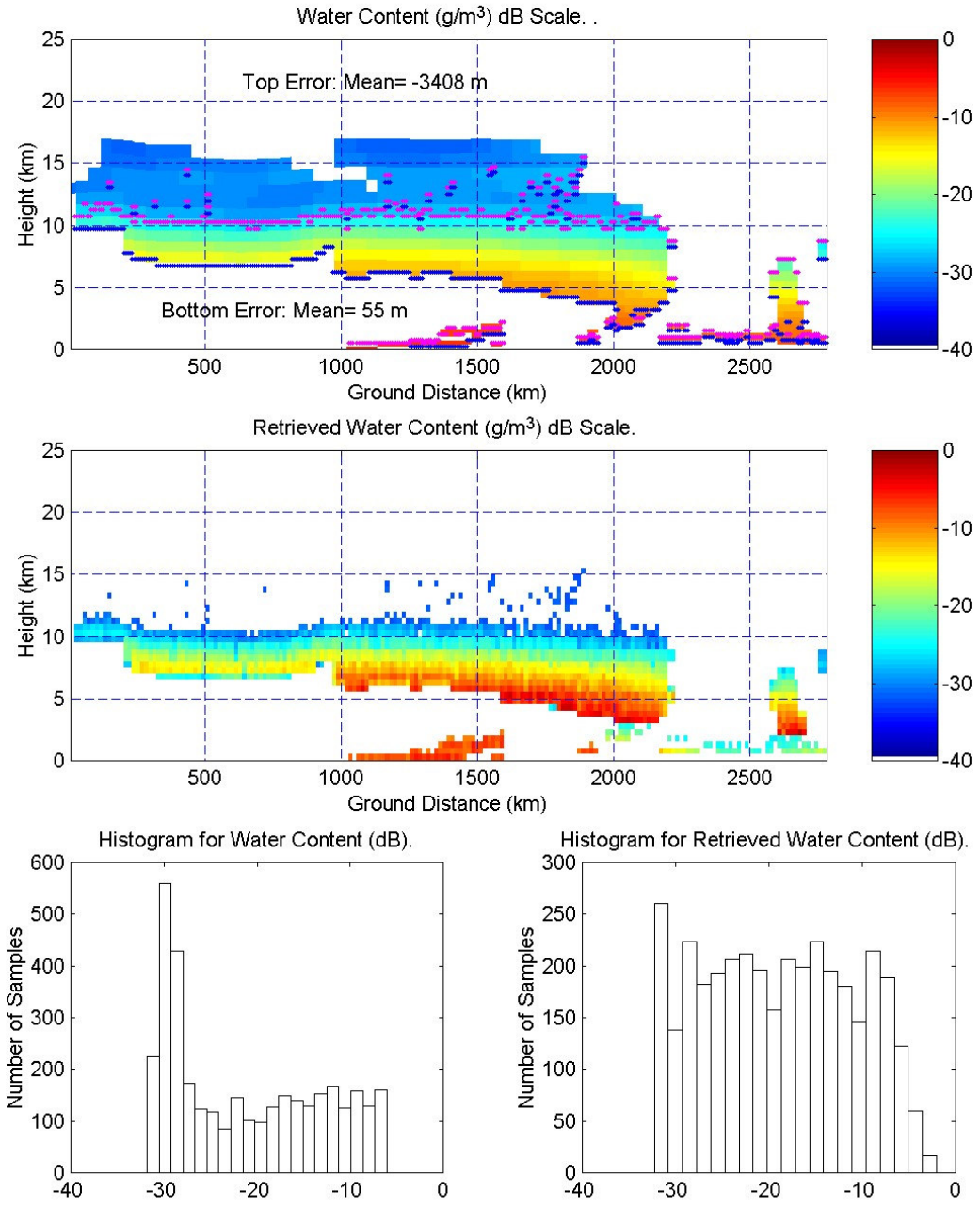

Figure A-2 Scene CLARE50km_16oct1998. **Upper panel**: Input Dataset Water Content along the trajectory at a resolution of 10.0 km. The cloud top and bottom, as retrieved by CPR, are shown by magenta and blue points respectively. **Center panel**: Retrieved Water Content. Attenuation compensation with knowledge of temperature profile has been used in the retrieval. **Lower panels**: Histograms for the Input Dataset and Retrieved Water Content.

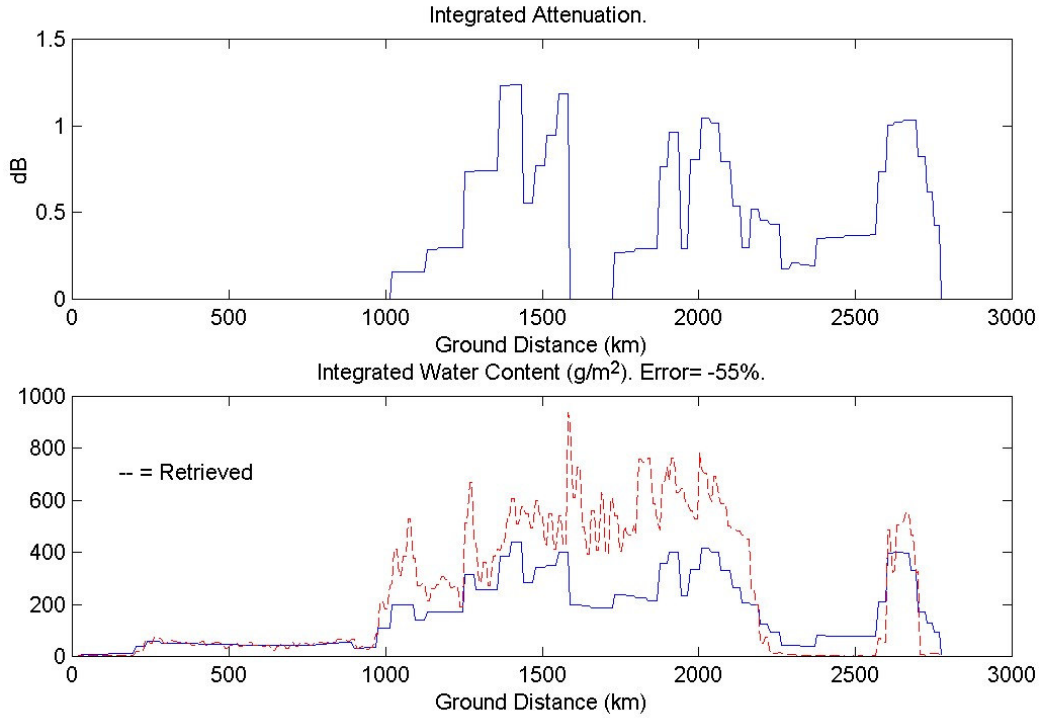

Figure A-3 Scene CLARE50km_16oct1998. **Upper panel**: Integrated Attenuation. It is the total attenuation down to the surface including cloud and atmosphere attenuation. **Lower panel**: Water content integrated along the vertical column. The red dotted line indicates the retrieved value and the blue continuous line is the true value.

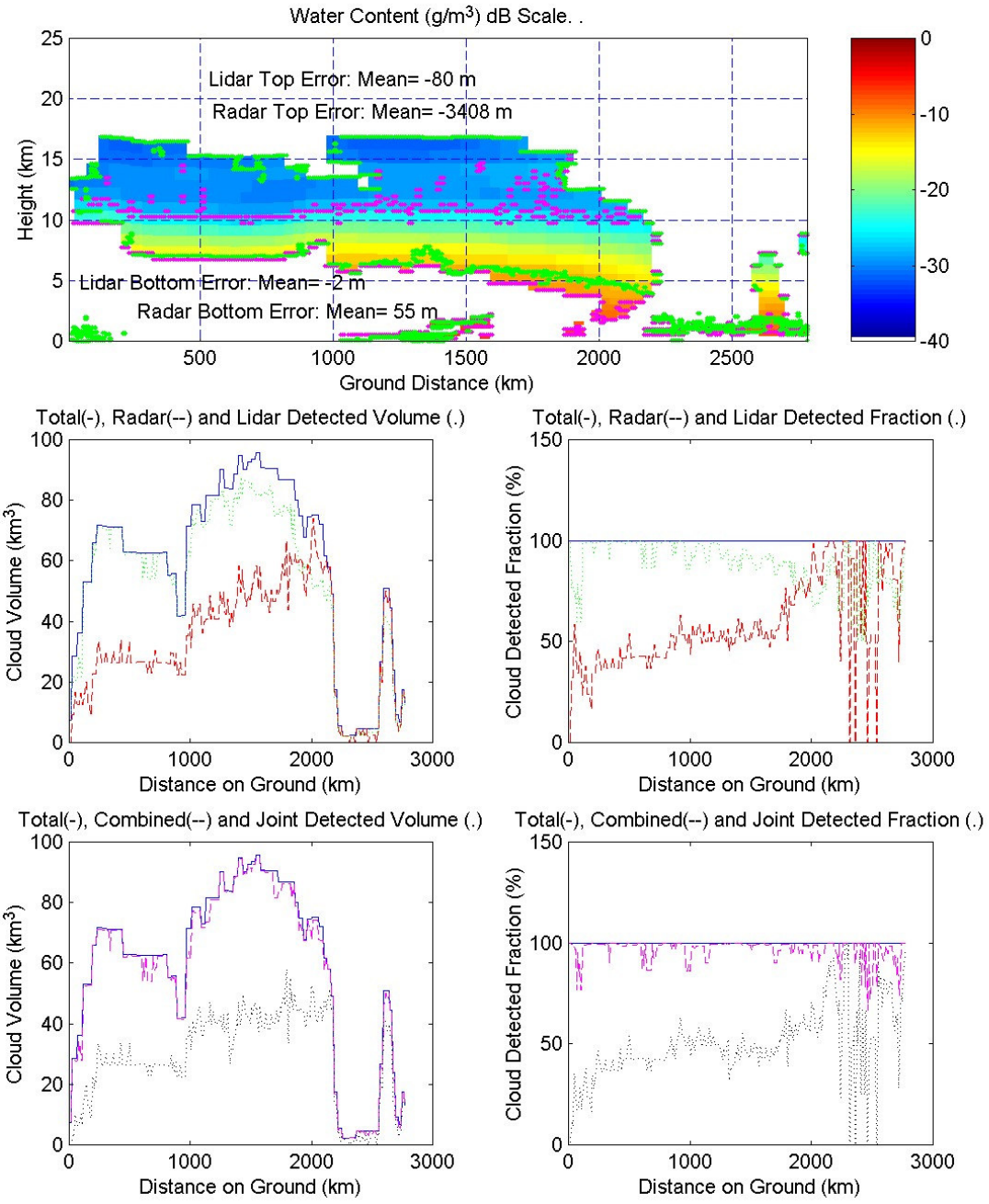

Figure A-4 Scene CLARE50km_16oct1998. **Upper panel**: Cloud Top and Bottom for Lidar (green dotted points) and Radar (magenta dotted points) superimposed to Water Content in the input dataset. **Lower panels (4)**: Combined Detection Statistics for Lidar and Radar. Blue line (true volume). Up panels: Dashed red line (radar), green points (lidar). Low panels: magenta and black lines are referred to combined and joint detected respectively.

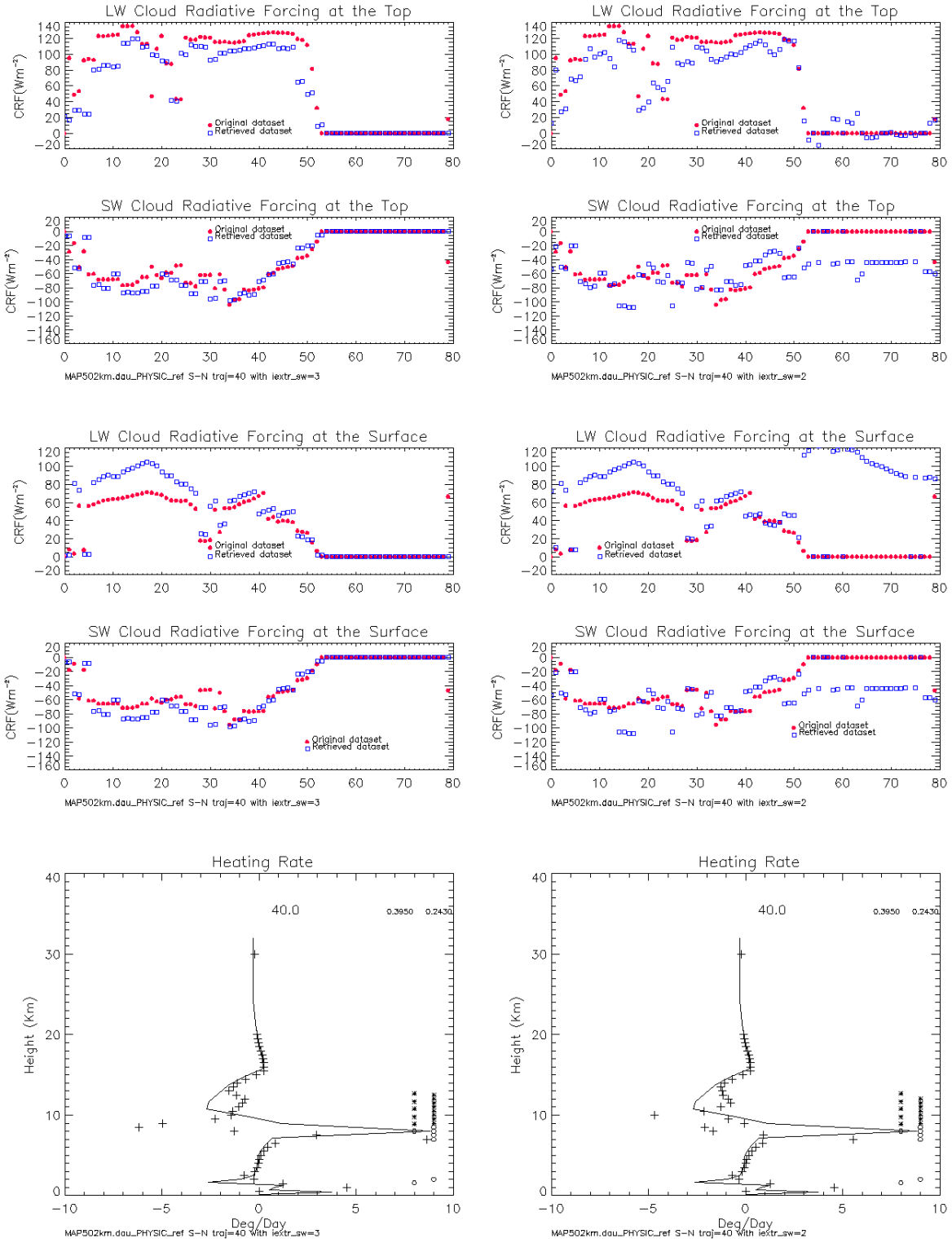

Figure A-5 MAP50km, S-N trajectory. Comparisons between retrieved and original datasets. On the left-hand-side only radar is used while on the right-hand-side, both radar and lidar are used in synergy. **4 upper panels**: LW and SW cloud radiative forcing at TOA and surface. **2 Lower panels**: Heating rate profile at position # 40.